The cone photoreceptor mosaic in aniridia: within-family phenotype-genotype discordance.

Hilde R.Pedersen[1] MaureenNeitz[2] Stuart J.Gilson[1] Erlend C.S.Landsend[3] Øygunn Aas Utheim[4] Tor PaaskeUtheim[13] Rigmor C.Baraas[1]

[1] National Centre for Optics, Vision and Eye Care, Faculty of Health and Social Sciences, University of South-Eastern Norway, Kongsberg, Norway

[2] Department of Ophthalmology, University of Washington, Seattle, Washington

[3] Department of Ophthalmology, Oslo University Hospital, Oslo, Norway

[4] The Norwegian Dry Eye Clinic, Oslo, Norway

Ophtalmology. 2019, *3(6)*, 523-534.
DOI: http://dx.doi.org10.1016/j.oret.2019.01.020

The Cone Photoreceptor Mosaic in Aniridia: Within-Family Phenotype-Genotype Discordance

Hilde R. Pedersen, MSc[1], Maureen Neitz, PhD[2], Stuart J. Gilson, PhD[1], Erlend C. S. Landsend, MD[3], Øygunn Aas Utheim, MD, PhD[4], Tor Paaske Utheim, MD, PhD[1,3] and Rigmor C. Baraas*, PhD[1]

[1]National Centre for Optics, Vision and Eye Care, Faculty of Health and Social Sciences, University of South-Eastern Norway, Kongsberg, Norway

[2]Department of Ophthalmology, University of Washington, Seattle, WA, USA

[3]Department of Ophthalmology, Oslo University Hospital, Oslo, Norway

[4]The Norwegian Dry Eye Clinic, Oslo, Norway

*Corresponding author
Address: University of South-Eastern Norway
National Centre for Optics, Vision and Eye Care
Hasbergsvei 36, 3616 Kongsberg, Norway
E-mail: rigmor.baraas@usn.no

Meeting Presentation: Part of the results was presented at the Association for Research in Vision and Ophthalmology (ARVO) annual meeting 2018, Honolulu, Hawaii, US and at the 4th European Conference on Aniridia 2018, Paris, France.

Financial support: Supported by the Norwegian Association of Aniridia (Aniridi Norge). The genetic analysis portion of this work was conducted by the University of Washington and was supported by Research to Prevent Blindness, and National Institutes of Health/National Eye Institute Grant P30EY001730. HRP holds a PhD position funded by the Norwegian Ministry of Education and Research.

Conflict of Interest: No conflicting relationship exists for any author

Running head: The cone photoreceptor mosaic in aniridia

Address for reprints: University of South-Eastern Norway, National Centre for Optics, Vision and Eye Care, Hasbergsvei 36, 3616 Kongsberg, Norway

This article contains additional online-only material. The following should appear online-only: Figure S1

Abstract

Purpose: Investigate *in-vivo* cone photoreceptor structure in familial aniridia caused by a deletion in the *PAX6* gene to elucidate the complexity of between-individual variation in retinal phenotype.

Design: Descriptive case-control study

Participants: Eight persons with congenital aniridia (5 males; aged 40–66) from one family and 33 normal controls (14 males, aged 14–69 yrs), including seven unaffected family members (3 males; aged 14–53yrs).

Methods: DNA was isolated from saliva samples and used in PCR to amplify and sequence exons and intron/exon junctions of the *PAX6* gene. Fluorescent DNA sequencing was performed on both DNA strands. High-resolution retinal images were acquired with Heidelberg Spectralis (SD-OCT2) and Adaptive optics scanning light ophthalmoscopy (AOSLO). Cone density (CD; cones/mm^2) and mosaic regularity were estimated along nasal-temporal meridians within the central 0–5° eccentricity. Horizontal SD-OCT line scans were segmented to analyze severity of foveal hypoplasia and measure retinal layer thicknesses.

Main Outcomes and Measures: Within-family variability in macular retinal layer thicknesses, cone photoreceptor density and mosaic regularity in aniridia compared with normal controls.

Results: DNA sequencing revealed a known *PAX6* mutation (IV2-2delA). Those with aniridia had variable iris phenotype ranging from almost normal appearance to no iris. Four with aniridia had FH grade 2, two had grade 3 and one had grade 4. Visual acuity ranged from

0.20–0.86 logMAR. AOSLO images were acquired of five family members with aniridia. Foveal CD varied between 19899 and 55128 cones/mm^2 with overlap between the foveal hypoplasia grades. CD was ≥3 SD below the normal mean within 0.5°, ≥2 SD below the normal mean at 0.5°–4°, and >1SD below the normal mean at 5° retinal eccentricity.

Conclusions: The results show considerable variability in foveal development within a family carrying the same *PAX6* mutation. This, together with the structural and functional variability within each grade of foveal hypoplasia, underlines the importance of advancing knowledge about retinal cellular phenotype in aniridia.

Congenital aniridia usually causes significant visual impairment. Bilateral hypoplasia of iris and fovea are characteristic findings. Persons with aniridia are at high risk of developing early onset cataract, keratopathy and glaucoma. Based on population studies in Norway, Sweden, Denmark and the US, the prevalence of aniridia is estimated to be 1:64000–1:96000.[1, 2] Heterozygous mutations in *paired box gene 6* (*PAX6)*[3] are primarily responsible for aniridia. Most known mutations introduce premature termination codons into the PAX6 open reading frame that lead to haploinsufficiency of the PAX6 transcription factor, either by mutations within the *PAX6* gene, its regulatory elements or more rarely by chromosomal deletions of band 11p13.[4, 5] Inheritance is typically autosomal dominant.[6] The phenotypic spectrum associated with *PAX6* mutations is extensive and aniridia is associated with considerable variability in phenotype and severity.[7]

The *PAX6* gene is a key regulator for normal eye development and interacts with many other genes and proteins. A network of transcription factors including PAX6 is expressed in retinal progenitor cells to control differentiation of multiple early- (i.e. retinal ganglion cells, cone photoreceptors) and late-born (glycinergic amacrine cells, bipolar cells) retinal nerve cell types.[8] Normal foveal development is characterized by formation of a foveal avascular zone (FAZ) before the foveal depression is formed and displacement of the inner retinal layers. Postnatal elongation and migration of cones toward the center of the fovea leads to a pronounced increase in cone photoreceptor density.[9-11] Aniridia associated mutations within the *PAX6* gene are known to alter retinal cell composition and subsequent post-receptoral organization including arrested formation of the fovea.[12-14] It is not known if the degree of PAX6 haploinsufficiency correlates with the degree of foveal hypoplasia[15] and impaired migration of cone photoreceptors towards the fovea center.[9-11]

Few studies have used high-resolution imaging to investigate retinal layer structure in aniridia,[13, 16] and none have investigated the cone photoreceptor mosaic. Here, spectral domain optical coherence tomography (SD-OCT) and adaptive optics scanning light ophthalmoscopy (AOSLO) were combined to advance the understanding of foveal hypoplasia in familial aniridia through *in vivo* examinations of retinal layers and photoreceptors at single-cell resolution. This allowed detailed evaluation of retinal phenotypic variability within a family with aniridia.

Methods

Participants

Eight persons from one family with congenital aniridia (5 males, aged 40–66 yrs) and 33 normal controls (14 males, aged 14–69 yrs), including seven unaffected family members (3 males, aged 14–53 yrs), were recruited through the Norwegian Association of Aniridia, via family members, or through the National Centre for Optics, Vision and Eye Care, University of South-Eastern Norway. The study was conducted in accordance with the principles in the Helsinki Declaration and approved by the Regional Committee for Medical and Health Research Ethics (Southern Norway Regional Health Authority). All participants and/or their guardians gave written informed consent after the purpose, procedures and possible consequences of the study were explained.

Genetic Analysis

DNA was extracted from saliva samples collected with the Oragene-DNA Self-Collection Kit, OG-500 (DNA Genotek Inc., Ottawa, ON, Canada) from all 41 participants. The *PAX6* gene was amplified and exon and intron/exon junctions sequenced using PCR primers and conditions described previously.[17] Fluorescent DNA sequencing was performed on both DNA strands. One family member with aniridia and three unaffected family members who gave saliva samples for genotyping were unable to participate in any further studies.

Clinical Assessment

Seven of eight family members with aniridia, four unaffected family members and 26 non-related normal controls underwent an eye examination including refraction, evaluation of anterior and posterior segment and ocular biometry (IOL Master, Carl Zeiss Meditec AG, Jena, Germany), as well as optical coherence tomography (details below). Visual acuity (logMAR) was measured with a digital high-contrast chart at 6 meters (TestChart 2000, Thompson Software Solutions, London, UK). The Lens Opacities Classification System III (LOCS III)[18] was used to evaluate the clarity of the lens. Aniridia associated keratopathy (AAK) was graded based on a previously described grading scale.[19]

Optical Coherence Tomography

High resolution volumetric SD-OCT images were acquired with the Heidelberg Spectralis OCT2 (Heidelberg Engineering GmbH, Heidelberg; Germany). The scans were 30x10 degrees, consisted of 49 B-scans (1536 A-scans/ B-scan) and were centred at the assumed foveal center. To improve signal-to-noise ratio and compensate for eye motion (TruTrack™, Heidelberg Engineering), 20 B-scans (frames) were averaged during acquisition. One eye, for which macular volumes could not be obtained because of severe nystagmus, was imaged using horizontal line scans with a nominal scan length of 30 degrees. Multiple scans were acquired in the foveal region to identify signs of foveal specialization.[9, 20, 21] The lateral scale of all OCT scans was corrected for retinal magnification factor based on individual ocular biometry, calculated with optical design software (Zemax EE, Radiant Zemax, Redmond, WA) using the Liou and Brennan eye model.[22]

SD-OCT-derived measures were obtained semi-automatically with custom software. An automatic active contour method,[23] using the Python implementation by van der Walt *et al.*,[24] was used to first segment the anterior edge at the inner limiting membrane (ILM) in a similar fashion as described by Mishra *et al.*.[25] Successive layers were then segmented at the posterior boundary of the outer plexiform layer (OPL), center of the external limiting membrane (ELM), ellipsoid zone (EZ) and interdigitation zone (IZ), and the posterior boundary RPE-Bruch's Membrane (RPE-BrM) band, using the contour of the previous layer as a seed. Foveal center was defined as the section with maximum outer segment length (EZ to IZ) and minimum foveal thickness (ILM to RPE-BrM) within the foveal pit. When no pit was present, the maximum lengthening of the photoreceptor outer segments (EZ to IZ) or/and

widening of the outer nuclear layer (OPL to ELM) was used to identify the expected foveal center. The B-scan through the defined foveal center was used for analysis.

The thickness values for each segmented layer were extracted and averaged at 5-pixel (≈28.3 µm) increments from the expected foveal center out to 10 degrees temporal and nasal eccentricity and thickness of each retinal layer was calculated. Definition of the retinal layers are presented in Figure 1A. Outer nuclear layer (ONL) and Henles fiber layer (HFL) was defined as one layer because the HFL could not easily be differentiated from the ONL without capturing directional OCT.[26] The relative foveal-to-perifoveal lengthening of the photoreceptor OS, IS and ONL+HFL was calculated by dividing their foveal thickness value by the average of their thickness at 5 degrees nasal and temporal to the fovea.

Adaptive Optics Scanning Light Ophthalmoscopy

The Kongsberg AOSLO[27, 28] was used to obtain images of the photoreceptor mosaic in five participants with aniridia (4 males, aged 40–66 yrs), and 30 age-matched normal controls including four unaffected family members. Ocular media opacities and nystagmus precluded imaging of the photoreceptor mosaic in participant 5114 and 5135. Before imaging, one drop of cyclopentolate 1% or tropicamide 0.5% was used to dilate the pupil and control accommodation in participants without severe iris hypoplasia. Confocal[29] and non-confocal split-detector[30] images with 1° fields of view were acquired simultaneously within one degree of the foveal location, and along the temporal and nasal meridians out to 5° eccentricity sampled at 0.5° or 1°-intervals. Individual raw image sequences contained 150 frames. Image analyses and registration was performed as described previously.[28] Registered

images from each retinal location were manually stitched together into a montage aligned with the corresponding en-face infrared image acquired by the OCT using selected blood vessel landmarks. These steps ensured that the AOSLO images were correctly scaled and positioned irrespective of the individual subject's fixation skill and uncontrolled eye movements. The image montages were cross-referenced with the OCT scans to confirm that the location of the foveal center corresponded in both modalities. This allowed us to estimate the location of the foveal center in the AOSLO montage also when the most central cones could not be reliably resolved.

Cone Density and Mosaic Regularity

Individual cones in the confocal images were identified via a semi-automatic algorithm as described previously.[28, 31] Non-confocal split-detection images were used to disambiguate cones from rods in the perifovea. Cone density was estimated over 50×50 µm sampling windows at the foveal center out to 5° eccentricity along the horizontal and nasal meridian. Voronoi analysis[32] was performed to measure inter cell distance (ICD; the average distance between a cone and all of its neighbors) and the average distance between each cone and its nearest neighbor (NND) for all cones whose Voronoi cell was completely contained within the sampling window.[33] The percentage of 6-sided Voronoi cells was calculated to characterize the regularity of the photoreceptor mosaic. The mean (µ) and SD (σ) for each metric was calculated to find the coefficient of variation (CV = σ/µ) to indicate the overall regularity of the ICD and NND independent of density and distance between the cones. Each participant’s dominant eye was used for OCT and AOSLO analysis.

Statistics

QQ-plots, histograms and the Shapiro-Wilk test were used to assess normality of the variables. Means ± SD are reported for the normal control data and full range for the aniridia data. Wilcoxon rank sum test (equivalent to the Mann-Whitney U test) was applied for independent samples. Correlations were assessed with Spearman correlation coefficients. Linear regression analysis was performed to investigate age-related changes in cone density for the normal controls. The significance level was set to $P \leq 0.05$. Statistical analyses were performed using R statistical software, version 3.5.1, including the package ggplot2.

Intra and inter-observer reliability

Intraclass correlation coefficients (ICC)[34] were computed to assess the intra and inter-rater reliability associated with cone density estimates in images of the foveal, para- and perifoveal cone mosaic in the participants with aniridia. The cone density measurements were repeated by two observers (authors HRP and RCB) at four retinal locations (foveal center, 1°, 3° and 5° retinal eccentricity) from each of the five participants with aniridia (total of 20 images). Agreement was assessed between the two observers, as well as between two measurements made by the same observer (author HRP). Analysis were performed using R statistical software, version 3.5.1, including the package “irr”. A one-way model, where only the subjects are considered as random effects, was considered appropriate.

Results

Clinical Findings and Genetics

DNA sequencing revealed an IV2-2delA mutation of the *PAX6* gene in eight of the family members who were previously diagnosed with aniridia. This mutation is known to cause aniridia and has been reported in the Human *PAX6* Allelic Variant Database (Leiden Open Variation Database, LOVD).[3] It is a deletion of the -2 nucleotide in intron 2, disrupting the canonical splice site sequence at the 3´ splice acceptor site upstream of exon 2. This mutation will affect splicing, most often resulting in exon skipping. However, this is a non-coding exon and the effect on the protein translation is not known, but may lead to loss of functional protein.[35] No *PAX6* abnormality was identified in the seven unaffected family members, nor in any of the other normal controls. The inheritance pattern of the mutation is shown in Figure S1(available as Supplemental material).

Table 1 shows a summary of clinical phenotype in the seven family members with aniridia who underwent an eye examination (marked with * in Figure S1).Total or near total iris hypoplasia, or a thin rim of iris were observed in six of the family members. Participant 5199 had, at first glance, a normal iris but was, on closer inspection, unusually thin and bright grey/pale blue and the pupil decentered nasally in both eyes (Figure 2A).

The normal controls, including the four unaffected family members, were healthy with no reported systemic disease or ocular abnormalities and were found to be free of eye disease upon clinical assessment including fundus examination. Visual acuity was 0.10 logMAR or better.

Retinal Layer Thicknesses and Foveal Cone Specialization

Foveal hypoplasia was observed in all participants with aniridia; four had grade 2 (all males), two had grade 3 (both females) and one had grade 4 (female). All, as per grading definition, lacked excavation of inner retinal layers, but ONL and cone outer segment thickness in the fovea varied considerably between and within each foveal hypoplasia grade (Figure 1).

Total foveal thickness (Figure 3A) ranged from 302.1–357.8 µm, compared with normal controls who had a mean ± SD foveal thickness of 230.3 ± 18.9 µm, $P < 0.001$. The foveal ONL+HFL thickness (Figure 3B) in aniridia ranged from 49.7–99.2 µm and was significantly thinner than in normal controls (mean 106.3 ± 14.8 µm, $P < 0.001$). Those with aniridia had shorter foveal cone outer segments (range 22.2–34.9 µm) compared with normal controls (mean 44.1 ± 3.3 µm, $P < 0.001$: Figure 3C). Relative lengthening (foveal:perifoveal length ratio) of the OS were, however, within normal mean ± 2SD for three of them, consistent with specialization of the foveal cones. The ONL+HFL and OS foveal:perifoveal length ratio show a clear relationship with foveal hypoplasia grade (Figure 3D). Those with aniridia had shorter IS length (range 26.9–34.6 vs mean ± SD 33.6 ± 2.4 µm) than the normal controls, but the difference was not significant (P =0 .08).

Retinal Cone Photoreceptor Density and Mosaic Regularity

Images of the foveal cone mosaic for those with aniridia and a normal control are shown in Figure 4 (*top*) together with confocal and split-detection images of para- and perifovea for one participant with aniridia (*bottom*). Peak cone density in aniridia ranged from 19899–55128 (38280 ± 14813) cones/mm^2 and was significantly reduced compared with normal

controls 91318–162282 (122231 ± 21572, n = 13) cones/mm^2 (P < 0.001). Peak cone density was not estimated in the normal controls where cones within the central 50×50 μm could not be reliably resolved.

The cone density topography among those with aniridia was similar in shape as seen in the normal controls, but with a flatter peak and reduced cone density at all retinal eccentricities within the central 10 degrees (Figure 5). Cone density varied between family members with aniridia and was ≥3 SD below the normal mean within 0.5°, ≥2 SD below the normal mean at 0.5°–4°, and >1SD below the normal mean at 5° retinal eccentricity. Estimates of cone density in the participants with aniridia showed a high intra-observer (ICC 0.991; 95% CI 0.977–0.996) and inter-observer agreement (ICC 0.989; 95% CI 0.972–0.996).

Cone mosaic regularity was measured by calculating the percentage of cones with six Voronoi cell neighbors. Those with aniridia had lower mean percentage Voronoi cells with six sides in the parafovea compared with normal controls (45.9 ± 10.0 % and 55.1 ± 9.9 %, respectively, P < 0.001), but not in the fovea (49.7 (35.3–67.0) % vs 52.0 ± 7.4%; Figure 6A). The eccentricity with comparable cone density to peak density in aniridia varies in normal controls, but for some it is at about 2.5° eccentricity, and the average ± SD percentage of six sided cells at this location is the same as that of the fovea: 52.1 ± 7.4%.

There was no difference in coefficients of variation in ICD at the foveal center between participants with aniridia (CV range = 0.091–0.144) and normal controls (CV mean ± SD = 0.107 ± 0.011, P = 0.57), however, overall variability in ICD was greater in aniridia (0.107 ± 0.022) than in normal retinas (0.086 ± 0.019, P < 0.001). This difference in coefficient of

variation was most evident in the parafovea (1–3° eccentricity; Figure 6B). The same trend was also observed in NND variability (Figure 6C).

Visual Function and Foveal Cone Specialization

The three females with FH grade 3–4 had the shortest OS (Figure 3C, filled symbols) and poorest VA, while all the four males had FH grade 2, longer OS and better VA. The two males with the best VA and red-green color sensitivity[14] had highest cone density, thickest ONL and longest OS (Figure 7). There was, however, an overlap in range of VA and cone density within the OCT grades (Table1). The oldest participant with aniridia, a male, had the lowest foveal cone density of all with aniridia, but his foveal cone outer segments were clearly elongated. His OS length and foveal:perifoveal OS ratio were similar to the other participants with FH grade 2 (Figure 3B), but he had a thinner ONL (Figure 3C). Moreover, there was evidence for cone packing towards the foveal center in the female with FH grade 4 even if no ONL or OS lengthening was observed on OCT images.

Sex Differences

The phenotype observed in the females with aniridia in this family were more severe than in the males; their degree of foveal hypoplasia was more severe; they had been diagnosed with glaucoma and two of the females had both optic nerve hypoplasia (ONH) and nystagmus (Table 1). None of the males had glaucoma, ONH or nystagmus. A sex difference was also observed between male and female controls with males having significantly thicker central retina (241.1 ± 21.1 vs 223.1 ± 13.6 µm, $P = 0.018$).

Discussion

This study shows the extent of phenotypic variability in familial aniridia through detailed *in-vivo* evaluation of iris and retinal structures of individuals carrying the same *PAX6* mutation. Compared to normal controls, greater central retinal thickness, shorter outer segments and thinner outer nuclear layer were observed in persons with aniridia. Cone density was reduced within the central 10 degrees, and the parafoveal cone mosaic was less regular in aniridia than normal retinas. In this particular family with aniridia, males were less affected than females. In addition to differences in severity of foveal hypoplasia, this difference was also evident in degree of iris hypoplasia, with one male having an almost normal iris, whereas all females had complete or nearly complete iris hypoplasia. Importantly, the poor association between iris and foveal hypoplasia underscores the importance of a thorough ocular examination for all members of families with aniridia, even those who initially appear unaffected.

The IVS2-delA mutation, found in all eight participants with aniridia, affects splicing in the 5´ untranslated region of the *PAX6* gene, probably excluding exon 3, but the effect on protein translation is unknown.[35, 36] The mutation, reported in the *PAX6* Allelic Variant Database, segregates with aniridia in a UK family and two sporadic cases in Russia and Germany.[3] Here, it was associated with a thinner outer nuclear layer and lower cone density than normal at all the measured eccentricities. Thus, the *PAX6* haploinsufficiency associated with this mutation results in a hypocellular retina, as a consequence of associated loss of propagation of retinal progenitor cells (RPC) and differentiation into different cell types early in development.[37-39] The lack of a foveal pit in FH grade 2 or more implies that retinal

development is arrested before the foveal pit normally starts to form, which is at mid-gestation (25–28 fetal weeks).[11, 21] Indeed, PAX6 is thought to play an indirect role on molecular markers that are normally expressed in retinal ganglion cells to prevent vascular ingrowth.[11] Foveal pit formation depends on the presence of a foveal avascular zone (FAZ) as well as an adequate proportion of midget-type ganglion cells to allow displacement of inner retinal layers.[10, 11]

The observed thinner outer retinal layers in those with aniridia, as compared with normal controls, is in line with impaired cone specialization. The foveal:perifoveal ratio (within normal range) of the ONL thickness and OS length (Figure 3D), however, suggests that some degree of foveal cone migration and specialization must have occurred even in persons with FH grade 2 and 3. This is further evidenced by similar foveal mosaic regularity in aniridia and controls, even if foveal cone density is significantly lower in aniridia. The observation suggests that cone packing has occurred independently of foveal pit formation which is in line with what Wilk *et al*.[40] propose in albinism; a foveal pit may not be needed for further cone packing, but plays a faciliatory role. The parafoveal cone mosaic was less regular in aniridia compared with controls, more akin to that observed for cones at greater eccentricities in normal retinas.

The degree of impaired migration and elongation of cones varied between FH grades as expected, but important differences were also observed within each FH grade. This may be a developmental difference related to the degree of vascularity in the deep foveal capillary plexus. This has been reported to contribute to the inhibition of outer retinal specialization.[41] Development of retinal vasculature in aniridia warrants further investigation. While the total number of cones in the retina is expected to remain constant

after mid-gestation,[21] early migration of cones towards the foveal center will increase the foveal cone density to a certain degree.[42] This initial cone migration may be responsible for the cone packing seen in the aniridia patients with lowest peak cone density. The visible foveal cone OS elongation and/or thickening of the ONL observed here in FH grade 2– 3, on the other hand, suggest that postnatal elongation and migration of cones have occurred in aniridia, but to a lesser degree than in normal controls. The observed cone packing towards the foveal center without ONL or OS lengthening in FH grade 4 may describe a threshold at which increased density will elongate cone OS. We have previously reported an association between foveal hypoplasia grade and red-green color discrimination in aniridia.[14] Here, higher foveal cone density was observed in those with the highest red-green sensitivity (lowest threshold) (Table 1). Differences in retinal ganglion cell (RGC) density and/or cone-RGC pathways[43] are factors that may explain variation in visual function between persons with the same grade of foveal hypoplasia and the variable relationship between CD, VA and color vision.

The two retinas with highest and the one with lowest CD in the aniridia group were both graded as FH grade 2. The age of the participant with lowest cone density may suggest an age-related decline in CD. A slight, but significant age-related decline in CD was also observed at 0.5˚ and 1˚ for the normal controls ($R^2 = 0.30$, $P = 0.001$ and $R^2 = 0.26$, $P = 0.002$, respectively); only three of the normal participants were older than 60 years. Pre-senile aging may play a role in aniridia together with additional factors (like increased vulnerability to retinal diseases due to the low redundancy of macular cones in foveal hypoplasia and possible risk for phototoxic damage). Subtle retinal changes and poorer image quality may also decrease the number of reflective cones that are identified in confocal AOSLO[44] and

thus underestimate cone density. Non-confocal images were unfortunately not available at this location for this participant.

In most cases, the phenotype in aniridia may be explained by the loss of one functional copy of the *PAX6* gene (haploinsufficiency), which provides an insufficient level of PAX6 protein.[4, 45] Abnormal mRNA is degraded through nonsense-mediated decay, which prevents accumulation of truncated protein products within cells.[46] It is not clear how haploinsufficiency can lead to wide variation in phenotype and severity within a family. However, the complex gene expression associated with PAX6 that is regulated at multiple levels during different processes of eye development, may contribute to large phenotypic variability.[47-49] Difference in genetic background, transcriptional and epigenetic regulation may alter the function of the PAX6 protein further, in turn affecting co-activators, co-repressors and regulation of downstream targets.[47, 50, 51] In some cases, competition for DNA-binding between truncated PAX6 proteins and wild-type PAX6 proteins possibly results in phenotypic variability, so-called dominant-negative effects.[52] It is not known if mutations that lead to abnormal mRNA splicing in the 5´UTR may cause this effect. In conclusion, quantitative analysis of cone elongation and packing within the macular area including the fovea allowed for a more detailed evaluation of retinal phenotypic variability in aniridia than reported previously. The analysis revealed decreased number of cones within the macular area and considerable variability in foveal development within a family with aniridia carrying the same genetic *PAX6* mutation. This, together with the structural and functional variability within each grade of foveal hypoplasia, underlines the importance of *in vivo* examinations of retinal layers and photoreceptors at single-cell resolution. Such detailed examinations are essential for improving our understanding of underlying pathophysiology and retinal

development in different aniridia *PAX6* mutations. This, to aid clinicians and scientists alike in determining prognosis, rehabilitation, and the potential for gene therapy and stem cell replacement strategies.

Data Availability

Access to relevant datasets are available at usn.figshare.com [https://doi.org/10.23642/usn.7605887].

References

1. Edén U, Iggman D, Riise R, Tornqvist K. Epidemiology of aniridia in Sweden and Norway. *Acta Ophthalmologica*. 2008;86:727-729.

2. Landsend ES, Utheim OA, Pedersen HR, Lagali N, Baraas RC, Utheim TP. The genetics of congenital aniridia-a guide for the ophthalmologist. *Surv Ophthalmol*. 2018;63:105-113.

3. Human PAX6 Allelic Variant Database (LOVD Database). http://lsdb.hgu.mrc.ac.uk/home.php?select_db=PAX6; Assessed August 18, 2018.

4. Vincent MC, Pujo AL, Olivier D, Calvas P. Screening for PAX6 gene mutations is consistent with haploinsufficiency as the main mechanism leading to various ocular defects. *Eur J Hum Genet*. 2003;11:163-169.

5. Kleinjan DA, Seawright A, Schedl A, Quinlan RA, Danes S, van Heyningen V. Aniridia-associated translocations, DNase hypersensitivity, sequence comparison and transgenic analysis redefine the functional domain of PAX6. *Human Molecular Genetics*. 2001;10:2049-2059.

6. Shaw MW, Falls HF, Neel JV. Congenital Aniridia. *Am J Hum Genet*. 1960;12:389-415.

7. Hingorani M, Williamson KA, Moore AT, van Heyningen V. Detailed ophthalmologic evaluation of 43 individuals with PAX6 mutations. *Invest Ophthalmol Vis Sci*. 2009;50:2581-2590.

8. Remez LA, Onishi A, Menuchin-Lasowski Y, et al. Pax6 is essential for the generation of late-born retinal neurons and for inhibition of photoreceptor-fate during late stages of retinogenesis. *Dev Biol*. 2017;432:140-150.

9. Yuodelis C, Hendrickson A. A qualitative and quantitative analysis of the human fovea during development. *Vision Res*. 1986;26:847-855.

10. Hendrickson A, Possin D, Vajzovic L, Toth CA. Histologic development of the human fovea from midgestation to maturity. *Am J Ophthalmol*. 2012;154:767-778.e762.

11. Provis JM, Dubis AM, Maddess T, Carroll J. Adaptation of the central retina for high acuity vision: cones, the fovea and the avascular zone. *Prog Retin Eye Res*. 2013;35:63-81.

12. Gregory-Evans K, Cheong-Leen R, George SM, et al. Non-invasive anterior segment and posterior segment optical coherence tomography and phenotypic characterization of aniridia. *Can J Ophthalmol*. 2011;46:337-344.

13. Sannan NS, Gregory-Evans CY, Lyons CJ, et al. Correlation of novel PAX6 gene abnormalities in aniridia and clinical presentation. *Can J Ophthalmol*. 2017;52:570-577.

14. Pedersen HR, Hagen LA, Landsend ECS, et al. Color Vision in Aniridia. *Investigative Ophthalmology & Visual Science*. 2018;59:2142-2152.

15. Thomas MG, Kumar A, Mohammad S, et al. Structural grading of foveal hypoplasia using spectral-domain optical coherence tomography a predictor of visual acuity? *Ophthalmology*. 2011;118:1653-1660.

16. Thomas S, Thomas MG, Andrews C, et al. Autosomal-dominant nystagmus, foveal hypoplasia and presenile cataract associated with a novel PAX6 mutation. *Eur J Hum Genet*. 2014;22:344-349.

17. Yokoi T, Nishina S, Fukami M, et al. Genotype-phenotype correlation of PAX6 gene mutations in aniridia. *Hum Genome Var*. 2016;3:15052.

18. Chylack LT, Jr., Wolfe JK, Singer DM, et al. The Lens Opacities Classification System III. The Longitudinal Study of Cataract Study Group. *Arch Ophthalmol*. 1993;111:831-836.

19. Landsend ECS, Pedersen HR, Utheim OA, et al. Meibomian gland dysfunction and keratopathy are associated with dry eye disease in aniridia. *Br J Ophthalmol*. 2018.

20. Dubis AM, Costakos DM, Subramaniam CD, et al. Evaluation of normal human foveal development using optical coherence tomography and histologic examination. *Arch Ophthalmol*. 2012;130:1291-1300.

21. Hendrickson AE, Yuodelis C. The morphological development of the human fovea. *Ophthalmology*. 1984;91:603-612.

22. Liou HL, Brennan NA. Anatomically accurate, finite model eye for optical modeling. *J Opt Soc Am A Opt Image Sci Vis*. 1997;14:1684-1695.

23. Kass M, Witkin A, Terzopoulos D. Snakes: Active contour models. *International Journal of Computer Vision*. 1988;1:321-331.

24. van der Walt S, Schonberger JL, Nunez-Iglesias J, et al. scikit-image: image processing in Python. *PeerJ*. 2014;2:e453.

25. Mishra A, Wong A, Bizheva K, Clausi DA. Intra-retinal layer segmentation in optical coherence tomography images. *Opt Express*. 2009;17:23719-23728.

26. Lujan BJ, Roorda A, Croskrey JA, et al. Directional optical coherence tomography provides accurate nuclear layer and Henle fiber layer measurements. *Retina*. 2015;35:1511-1520.

27. Dubra A, Sulai Y. Reflective afocal broadband adaptive optics scanning ophthalmoscope. *Biomed Opt Express*. 2011;2:1757-1768.

28. Pedersen HR, Gilson SJ, Dubra A, Munch IC, Larsen M, Baraas RC. Multimodal imaging of small hard retinal drusen in young healthy adults. *Br J Ophthalmol*. 2018;102:146-152.

29. Dubra A, Sulai Y, Norris JL, et al. Noninvasive imaging of the human rod photoreceptor mosaic using a confocal adaptive optics scanning ophthalmoscope. *Biomed Opt Express*. 2011;2:1864-1876.

30. Scoles D, Sulai YN, Langlo CS, et al. In vivo imaging of human cone photoreceptor inner segments. *Invest Ophthalmol Vis Sci*. 2014;55:4244-4251.

31. Li KY, Roorda A. Automated identification of cone photoreceptors in adaptive optics retinal images. *J Opt Soc Am A Opt Image Sci Vis*. 2007;24:1358-1363.

32. Baraas RC, Carroll J, Gunther KL, et al. Adaptive optics retinal imaging reveals S-cone dystrophy in tritan color-vision deficiency. *J Opt Soc Am A Opt Image Sci Vis*. 2007;24:1438-1447.

33. Cooper RF, Wilk MA, Tarima S, Carroll J. Evaluating Descriptive Metrics of the Human Cone Mosaic. *Invest Ophthalmol Vis Sci*. 2016;57:2992-3001.

34. Bland JM, Altman DG. Measurement error and correlation coefficients. *Bmj*. 1996;313:41-42.

35. Prosser J, van Heyningen V. PAX6 mutations reviewed. *Hum Mutat*. 1998;11:93-108.

36. Axton RA, Hanson IM, Love J, Seawright A, Prosser J, van Heyningen V. Combined SSCP/heteroduplex analysis in the screening for PAX6 mutations. *Mol Cell Probes*. 1997;11:287-292.

37. Oron-Karni V, Farhy C, Elgart M, et al. Dual requirement for Pax6 in retinal progenitor cells. *Development*. 2008;135:4037-4047.

38. Marquardt T, Ashery-Padan R, Andrejewski N, Scardigli R, Guillemot F, Gruss P. Pax6 is required for the multipotent state of retinal progenitor cells. *Cell*. 2001;105:43-55.

39. Klimova L, Kozmik Z. Stage-dependent requirement of neuroretinal Pax6 for lens and retina development. *Development*. 2014;141:1292-1302.

40. Wilk MA, McAllister JT, Cooper RF, et al. Relationship between foveal cone specialization and pit morphology in albinism. *Invest Ophthalmol Vis Sci*. 2014;55:4186-4198.

41. Pakzad-Vaezi K, Keane PA, Cardoso JN, Egan C, Tufail A. Optical coherence tomography angiography of foveal hypoplasia. *Br J Ophthalmol*. 2017;101:985-988.

42. Diaz-Araya C, Provis JM. Evidence of photoreceptor migration during early foveal development: a quantitative analysis of human fetal retinae. *Vis Neurosci*. 1992;8:505-514.

43. Rossi EA, Roorda A. The relationship between visual resolution and cone spacing in the human fovea. *Nat Neurosci*. 2010;13:156-157.

44. Pallikaris A, Williams DR, Hofer H. The reflectance of single cones in the living human eye. *Invest Ophthalmol Vis Sci*. 2003;44:4580-4592.

45. Lee HJ, Colby KA. A review of the clinical and genetic aspects of aniridia. *Semin Ophthalmol*. 2013;28:306-312.

46. Khajavi M, Inoue K, Lupski JR. Nonsense-mediated mRNA decay modulates clinical outcome of genetic disease. *European Journal Of Human Genetics*. 2006;14:1074.

47. Osumi N, Shinohara H, Numayama-Tsuruta K, Maekawa M. Concise review: Pax6 transcription factor contributes to both embryonic and adult neurogenesis as a multifunctional regulator. *Stem Cells*. 2008;26:1663-1672.

48. Hever AM, Williamson KA, van Heyningen V. Developmental malformations of the eye: the role of PAX6, SOX2 and OTX2. *Clin Genet*. 2006;69:459-470.

49. Cvekl A, Callaerts P. PAX6: 25th anniversary and more to learn. *Exp Eye Res*. 2017;156:10-21.

50. Ashery-Padan R, Marquardt T, Zhou X, Gruss P. Pax6 activity in the lens primordium is required for lens formation and for correct placement of a single retina in the eye. *Genes Dev*. 2000;14:2701-2711.

51. Gregory-Evans CY, Wallace VA, Gregory-Evans K. Gene networks: dissecting pathways in retinal development and disease. *Prog Retin Eye Res*. 2013;33:40-66.

52. Singh S, Tang HK, Lee JY, Saunders GF. Truncation mutations in the transactivation region of PAX6 result in dominant-negative mutants. *J Biol Chem*. 1998;273:21531-21541.

Figure legends

Figure 1: SD-OCT images of different degrees of foveal hypoplasia.

(A) Horizontal transfoveal OCT scan of a normal healthy 23 year old including a graphical illustration of the definition of the segmented retinal layers used in B–I. Foveal hypoplasia was graded according to Thomas *et al*.[15] as (B–E) grade 2, (F–G) grade 3, (H) grade 4 and (I) normal. (B–H) the variation in foveal hypoplasia in 7 family members with aniridia and (I) one unaffected family member. Arrows mark the location of the foveal center. This corresponds to the foveal location in the cone mosaics shown in Figure 4. Scale bars = 200 µm.

Figure 2: Iris and SD-OCT images of variation in iris phenotype. (A–G) Iris in participants carrying the *PAX6* mutation. (H) Iris in a normal control. (A) Iris with an almost normal appearance, but a slightly decentered pupil and thinning of the iris tissue. (B & D) Thin rim of remnant iris. (C & G) Almost total iris hypoplasia with only a small stump of visible remnant iris. (E & F) Total absence of iris. White arrows indicate the location of the iris structure in the corresponding OCT image shown in the right column

Figure 3: Variation in retinal layer thicknesses along the horizontal meridian in aniridia compared with normal controls. (A) Total retinal thickness, (B) outer nuclear layer thickness and (C) outer segment length. Black solid lines and the shaded area represent the normal mean ± 2 SD. The different filled symbols represent each of the three females with aniridia and foveal hypoplasia grade 3–4 (cf. Fig. 1 F–H). Open symbols/asterisk represent the four males with aniridia and FH grade 2 (cf. Fig 1 B–E). Relative lengthening of the foveal OS, IS and ONL+HFL represented as the foveal:perifoveal ratio is shown in (D). The normal mean is plotted as a horizontal bar with error bars representing ± 2 SD.

Figure 4: Adaptive optics scanning light ophthalmoscopy confocal and split-detection images show variability in foveal cone mosaic within the same aniridia *PAX6* genotype. (*Top*) Foveal AOSLO images with a 0.5°×0.5° field of view are shown for the five family members with aniridia and one unaffected family member (5159). Asterisks mark the location of the foveal center for each person. (*Bottom*) Image montage from the left eye of participant 5120. Nasal is toward the left and temporal is toward the right. AOSLO images 5120 and A-C corresponds to the locations indicated by the yellow squares (at ≈ 1°, 3° and 5° temporal eccentricity). (A_1, B_1, C_1) are confocal images, whereas (A_2, B_2, C_2) are non-confocal split detection images of the same locations. Scale bars = 20 µm.

Figure 5: Variation in cone density as a function of retinal eccentricity along the nasal and temporal meridian. (A) Five individuals with aniridia compared with mean ± SD cone density in 30 normal controls. (B–D) Cone density is re-plotted to show differences between normal controls and aniridia for three different age groups.

Figure 6: Photoreceptor mosaic regularity as a function of retinal eccentricity. (A) Percentage of six-sided Voronoi cells. (B) Variability in inter cone distance. (C) Variability in nearest neighbor distance. Each metric is plotted as a function of retinal eccentricity along the nasal and temporal meridian for five individuals with aniridia compared with mean ± SD of 30 normal controls. The variability in ICD and NND were calculated as coefficient of variation ($CV = \sigma/\mu$).

Figure 7: Relationship between foveal cone density and cone outer segment elongation. Peak cone density is plotted as a function of OS length. The different red symbols represent participants with aniridia and filled black circles are normal controls.

Precis

High-resolution *in-vivo* retinal imaging revealed decreased number of cones within the macular area in aniridia, but considerable between-individual variability in foveal development in family members carrying the same genetic *PAX6* mutation.

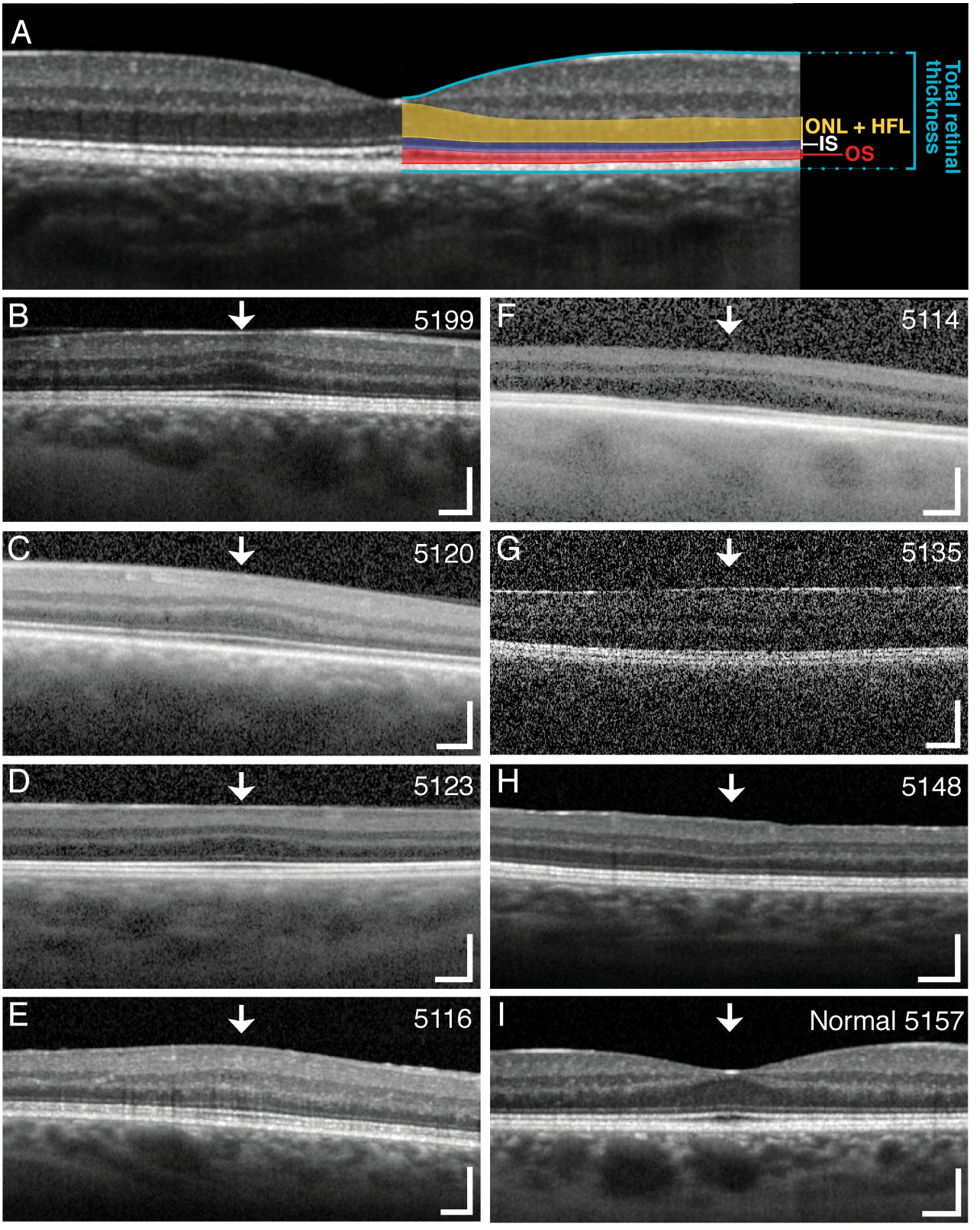
A
Total retinal thickness
ONL + HFL
IS
OS
B
5199
F
5114
C
5120
G
5135
D
5123
H
5148
E
5116
I
Normal 5157

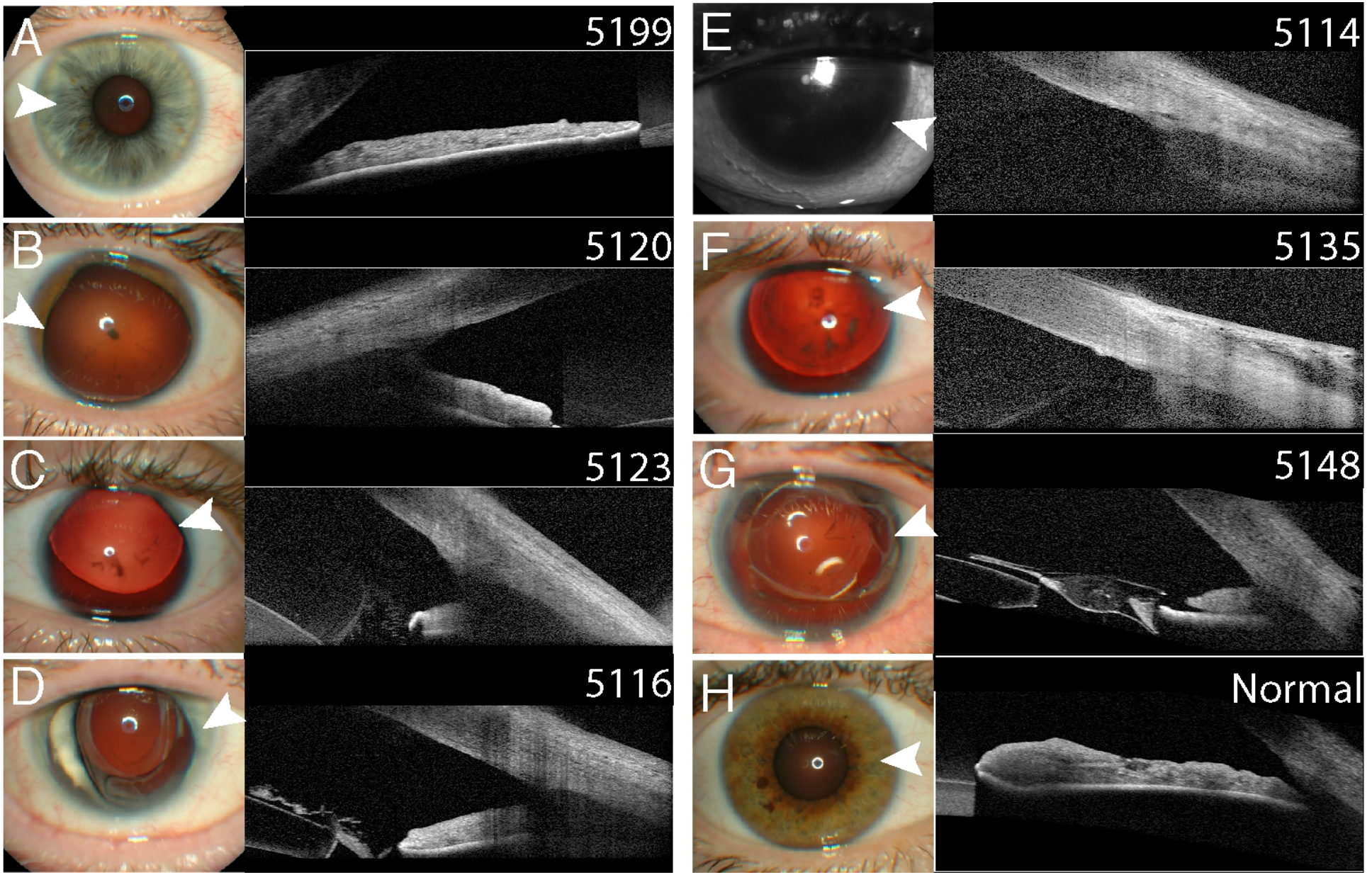
A
5199
B
5120
C
5123
D
5116
E
5114
F
5135
G
5148
H
Normal

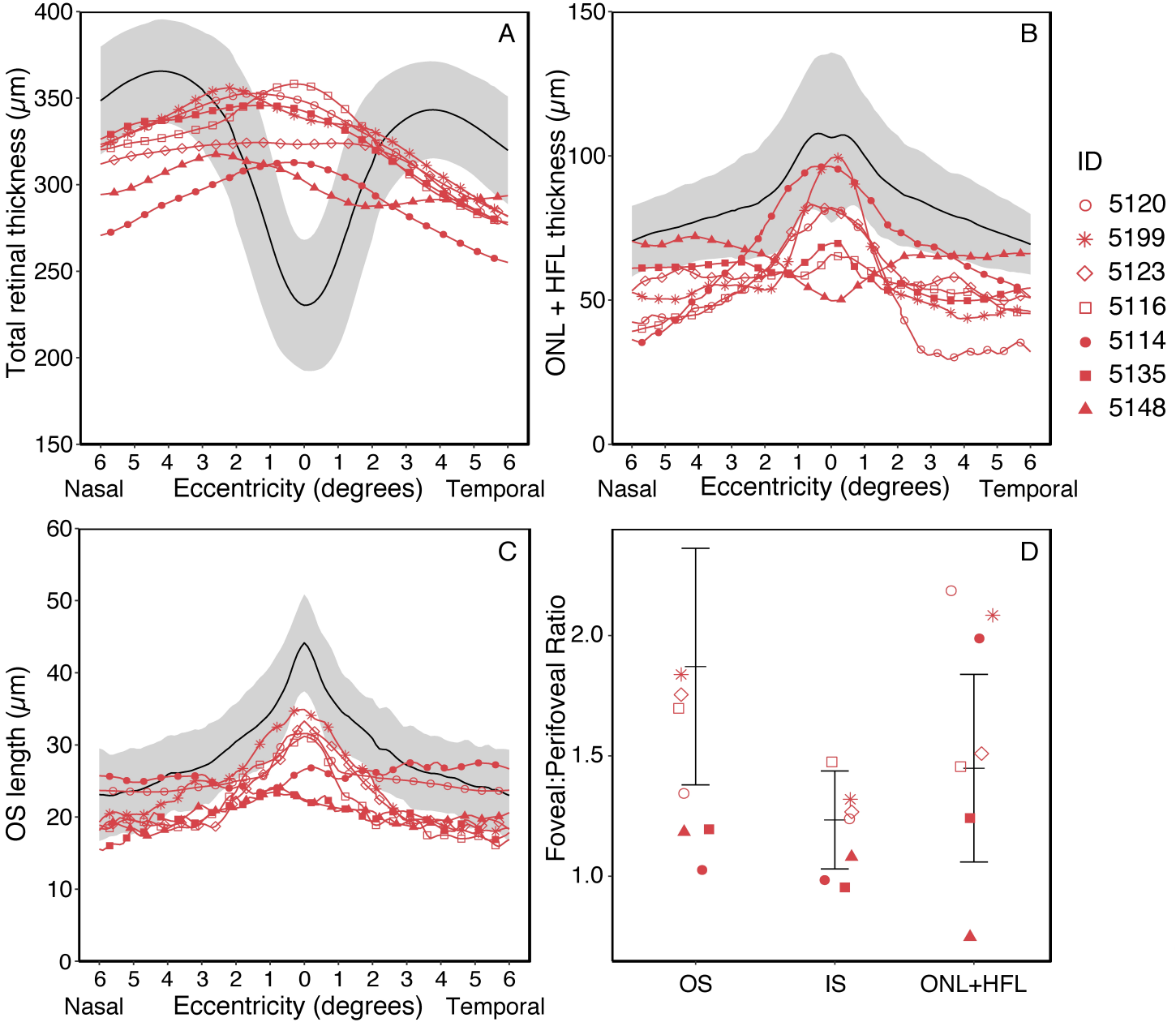
A
Total retinal thickness (μm)
400
350
300
250
200
150
6 5 4 3 2 1 0 1 2 3 4 5 6
Nasal
Eccentricity (degrees)
Temporal
B
ONL + HFL thickness (μm)
150
100
50
0
6 5 4 3 2 1 0 1 2 3 4 5 6
Nasal
Eccentricity (degrees)
Temporal
ID
5120
5199
5123
5116
5114
5135
5148
C
OS length (μm)
60
50
40
30
20
10
0
6 5 4 3 2 1 0 1 2 3 4 5 6
Nasal
Eccentricity (degrees)
Temporal
D
Foveal:Perifoveal Ratio
2.0
1.5
1.0
OS
IS
ONL+HFL

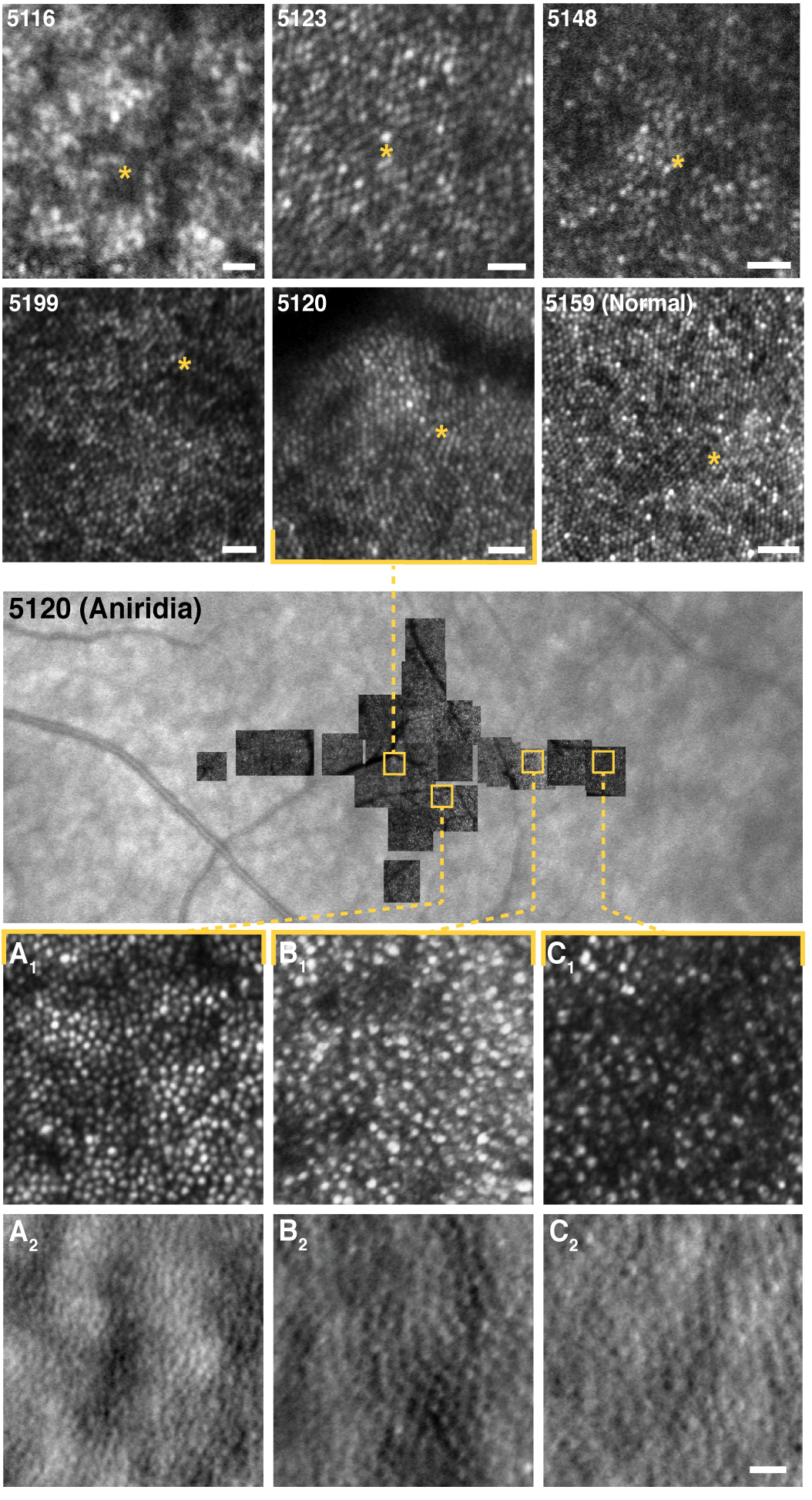
5116
5123
5148
5199
5120
5159 (Normal)
5120 (Aniridia)
A1
B1
C1
A2
B2
C2

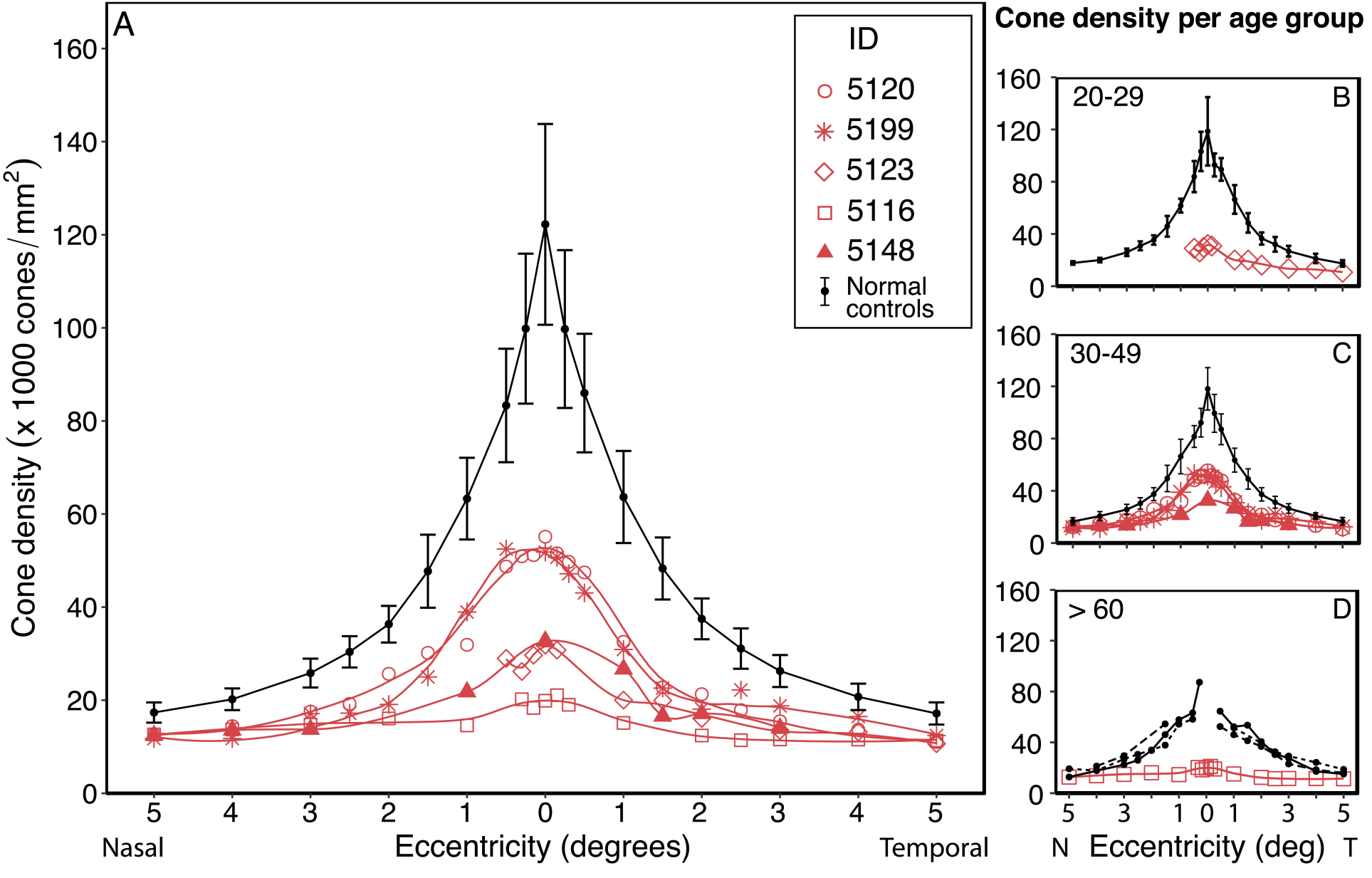
A
ID
5120
5199
5123
5116
5148
Normal controls
Cone density (x 1000 cones/mm^2)
Nasal
Eccentricity (degrees)
Temporal
Cone density per age group
20-29
B
30-49
C
> 60
D
N
Eccentricity (deg)
T

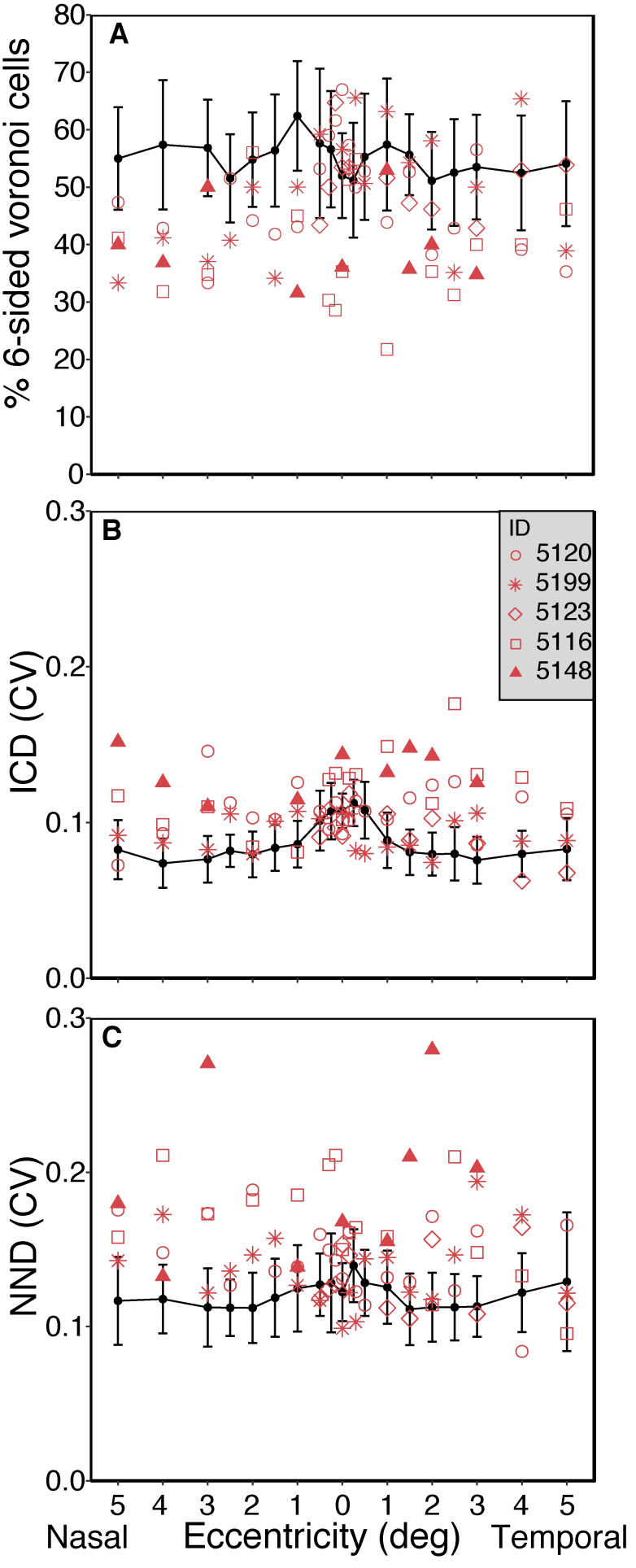
A
% 6-sided voronoi cells
80
70
60
50
40
30
20
10
0
B
ICD (CV)
0.3
0.2
0.1
0.0
ID
5120
5199
5123
5116
5148
C
NND (CV)
0.3
0.2
0.1
0.0
5 4 3 2 1 0 1 2 3 4 5
Nasal
Eccentricity (deg)
Temporal

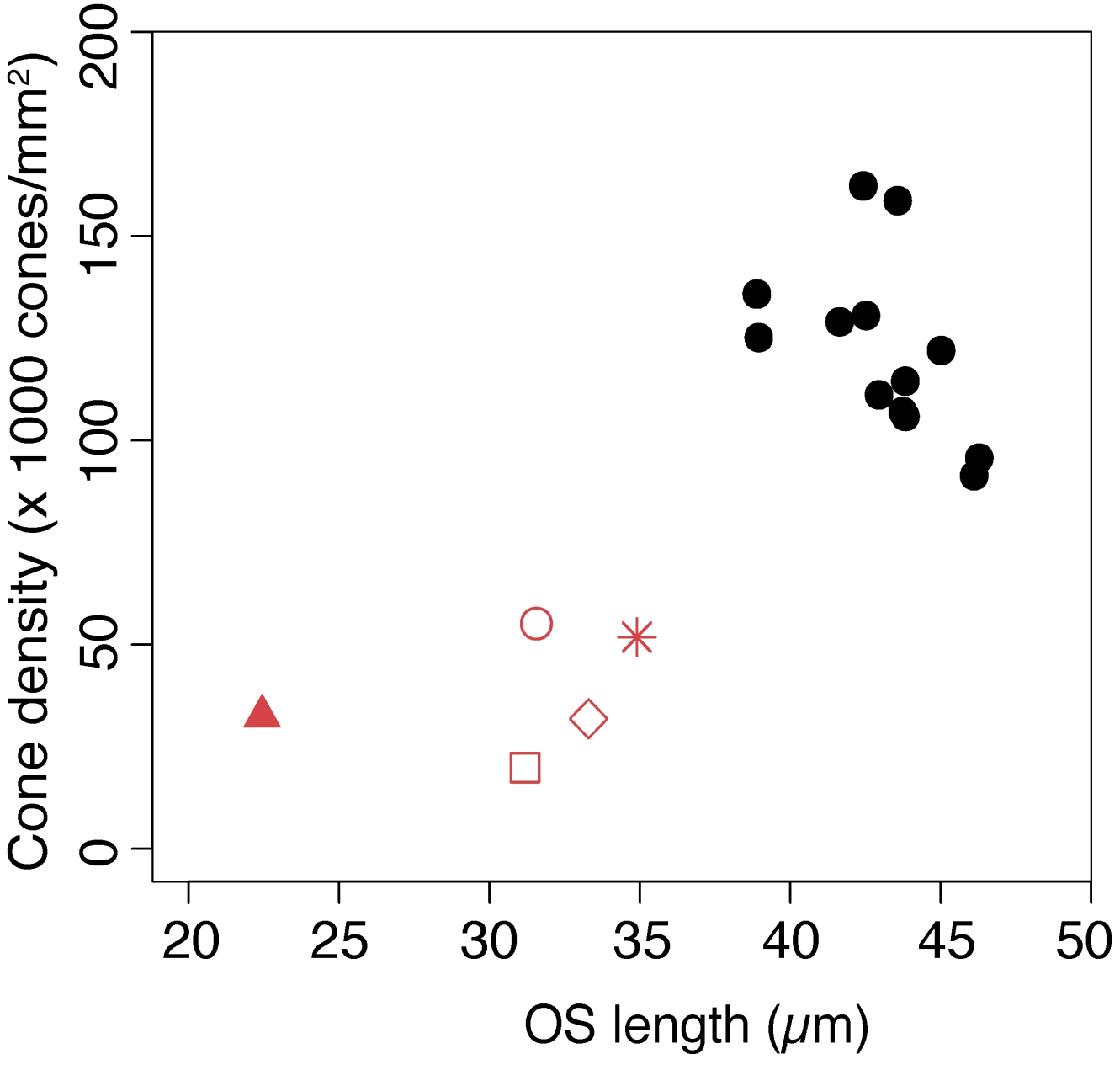
Cone density (x 1000 cones/mm²)
0
50
100
150
200
20
25
30
35
40
45
50
OS length (μm)

Table 1: Summary of clinical phenotype in the family members with a *PAX6* IV2-2delA mutation

ID	Age	Sex	Visual acuity [logMAR]	Axial length	Iris hypoplasia	Lens status	Nystagmus	AAK[a] grade	Glaucoma	Optic nerve hypoplasia	Foveal hypoplasia grade	CAD-LV[b] RG[c] Threshold[d]	Foveal cone density [cones/mm^2]	Symbol
5120	42	M	0.22	23.80	Thin rim of iris	N2, C1, P1	No	1	No	No	2	50	55128	○
5199	40	M	0.20	25.55	Bright iris, eccentric pupil	N0, C2, P0	No	1	No	No	2	78	51826	✳
5123	24	M	0.50	22.72	Almost complete	N1, C3, P1	No	2	No	No	2	118	31837	◇
5116	66	M	0.40	25.66	Thin rim of iris	Pseudo-phakic	No	2	No	No	2	116	19899	□
5114	56	F	0.86	23.97	Complete	Aphakic	Yes	1	Yes	Yes	3	434	NA	●
5135	40	F	0.70	24.05	Complete	N2, C4, P3	Yes	1	Yes	Yes	3	123	NA	■
5148	49	F	0.60	21.04	Almost complete	Pseudo-phakic	No	2	Yes	No	4	192	32713	▲

[a]AAK = Aniridia-associated keratopathy; [b]CAD-LV = low vision version of the Color Assessment and Diagnosis test; [c]RG = red-green; [d]Values derived from data collected by Pedersen *et al*.[14]

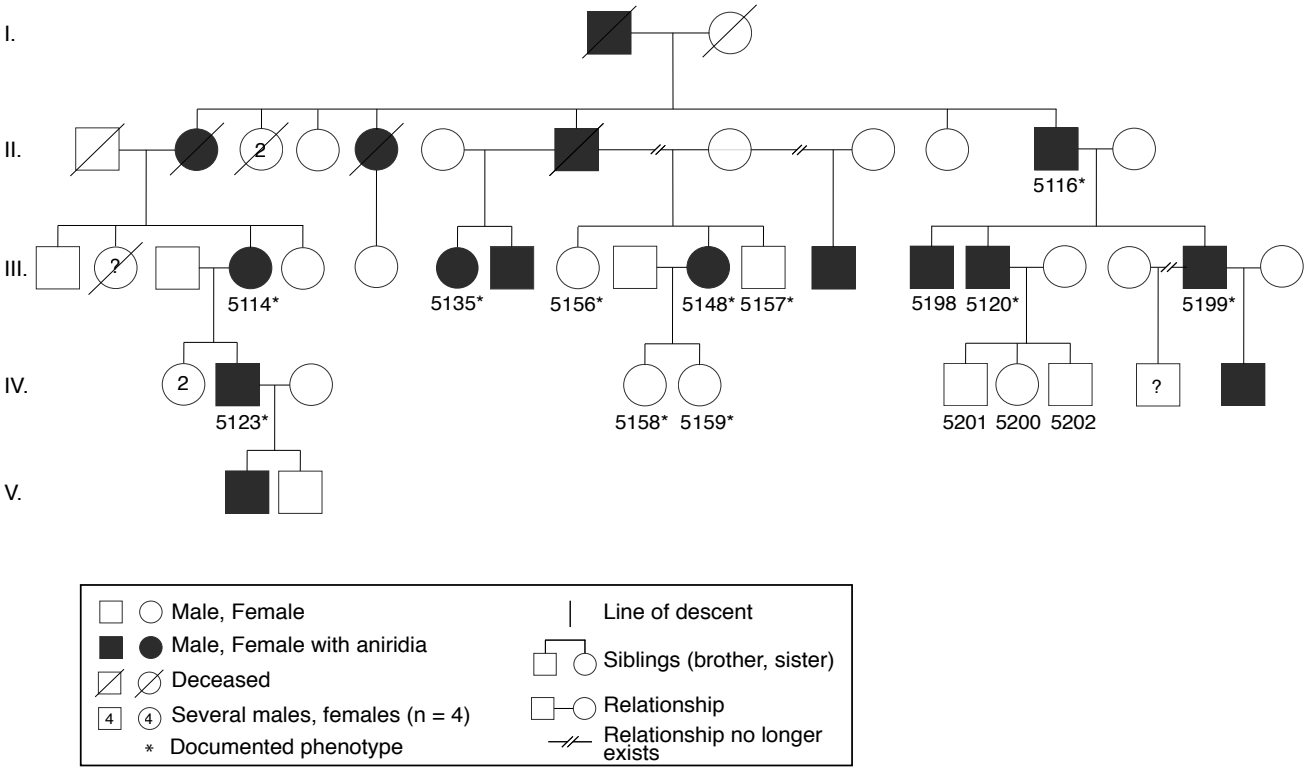

Figure S1: Pedigree of the family with a *PAX6* mutation showing an autosomal dominant inheritance pattern. The genotype was analyzed for 15 family members, indicated by their study ID number. The phenotype was documented for family members marked with study ID number followed by *. Written informed consent to publish the pedigree have been obtained from all the study participants and/or their guardians.